



## Dechlorination and defluorination capability of sulfidized nanoscale zerovalent iron with suppressed water reactivity

Zhen Cao<sup>a</sup>, Jiang Xu<sup>b,\*</sup>, Hao Li<sup>c</sup>, Tianyi Ma<sup>d</sup>, Liping Lou<sup>a</sup>, Graeme Henkelman<sup>c</sup>, Xinhua Xu<sup>a,\*</sup>

<sup>a</sup> Department of Environmental Engineering, Zhejiang University, Hangzhou 310058, China

<sup>b</sup> Department of Civil and Environmental Engineering, Carnegie Mellon University, Pittsburgh, PA 15213, USA

<sup>c</sup> Department of Chemistry and the Oden Institute for Computational Engineering and Sciences, The University of Texas at Austin, Austin, TX 78712, USA

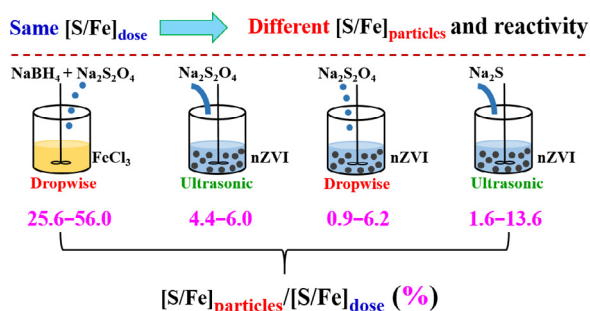
<sup>d</sup> Discipline of Chemistry, School of Environmental and Life Science, University of Newcastle, Callaghan, NSW 2308, Australia



### HIGHLIGHTS

- Sulfidation method affected the Fe<sup>0</sup> content and Fe crystalline structure.
- Sulfidation method affected the S speciation and distribution.
- Co-sulfidized S-nZVI incorporated more sulfur than post-sulfidized S-nZVI.
- S-in-Fe(1 1 0) can block more H adsorption sites than S-on-Fe(1 1 0).
- Sulfidation blocked the H<sub>2</sub> evolution and enhanced the florfenicol dehalogenation.

### GRAPHICAL ABSTRACT



### ARTICLE INFO

#### Keywords:

Sulfur content and speciation  
Sulfur reagents  
Density functional theory  
H<sub>2</sub> evolution  
Defluorination

### ABSTRACT

Recently, sulfidation of nanoscale zerovalent iron (S-nZVI) has become a potential remediation technology. However, the impact of sulfidation methods and actual sulfur content ( $[S/Fe]_{\text{particle}}$ ) on the physicochemical properties and the reactivity of S-nZVI remains unknown. Here, we synthesized S-nZVI via one co-sulfidation and three post-sulfidation methods to determine how different sulfur reagents and addition procedures affect the reactivity of S-nZVI for defluorination. The measured S amounts of co-sulfidized S-nZVI and post-sulfidized S-nZVI was much lower than their dose. Different sulfur reagents and sulfidation approach would affect the amount and speciation of sulfur in the particles. Sulfidation of nZVI improved the reactivity for dechlorination (up to 12-fold) and defluorination (up to 3-fold) of florfenicol (FF), but inhibited the reactivity with water (up to 31-fold). Density functional theory calculations showed that sulfidation increases the hydrophobicity of materials, and the amount and nature of sulfur affect the hydrophobicity and the number of blocked H sites. S-nZVI particles with more S<sup>2-</sup> and S<sub>2</sub><sup>2-</sup> species showed faster dechlorination and defluorination of FF. Up to ~45% of FF was defluorinated by S-nZVI after 15 days reaction at room temperature and pressure. The  $[S/Fe]_{\text{particle}}$  and Fe<sup>0</sup> content was responsible for the initial and long-term defluorination, respectively. These results suggest that S-nZVI could be a promising agent for defluorination, and the sulfur reagents and sulfidation approach would affect its properties and reactivity.

\* Corresponding authors.

E-mail addresses: [jiangx2@andrew.cmu.edu](mailto:jiangx2@andrew.cmu.edu) (J. Xu), [xuxinhua@zju.edu.cn](mailto:xuxinhua@zju.edu.cn) (X. Xu).

<https://doi.org/10.1016/j.cej.2020.125900>

Received 23 March 2020; Received in revised form 11 June 2020; Accepted 12 June 2020

Available online 17 June 2020

1385-8947/ © 2020 Elsevier B.V. All rights reserved.

## 1. Introduction

Nanoscale zero-valent iron (nZVI) has been widely studied due to its high reactivity towards halogenated organic pollutants, heavy metals, and other inorganic pollutants [1–9]. However, rapid aggregation and passivation of nZVI particles reduce its reactivity and mobility during *in-situ* remediation [10–13]. Meanwhile, the side reaction with water consumes  $\text{Fe}^0$  ( $\text{Fe}^0 + 2\text{H}_2\text{O} \rightarrow \text{Fe}^{2+} + 2\text{OH}^- + \text{H}_2$ ) and forms an iron oxide layer on the surface, reduces electron utilization, and leads to a shortening of reactive life [14]. Numerous efforts have been made to increase the reactivity of nZVI for decades, such as doping a noble metal (e.g. Pd and Ni) onto nZVI [15–17] and loading nZVI particles onto carbon supports or stabilizing nZVI particles with polymers [18–22]. Nevertheless, these methods cannot inhibit the side reaction between  $\text{Fe}^0$  and water, and will shorten the reactive lifetime of nZVI in water due to its larger surface area after stabilization.

Recently, sulfidation of nZVI has drawn interest for environmental remediation [23–26]. Sulfidized nZVI (S-nZVI) has been proposed to slow the side reaction between  $\text{Fe}^0$  and water, enhance the reactivity, extend the lifetime of the materials, and improve the electron selectivity for targeted contaminants [24,27–30]. To date, S-nZVI is synthesized via either a co-sulfidation method or a post-sulfidation method [31–33]. A typical co-sulfidation method uses the dropwise addition of a mixture of  $\text{Na}_2\text{S}_2\text{O}_4$  and  $\text{NaBH}_4$  solution into a  $\text{Fe}^{2+}$  or  $\text{Fe}^{3+}$  solution to directly form S-nZVI [32], while a typical post-sulfidation method involves synthesizing nZVI first, then adding a  $\text{Na}_2\text{S}$  solution into the nZVI suspension [33,34]. The effects of sulfidation on the nZVI reactivity has been correlated with the dosed S/Fe molar ratio ( $[\text{S}/\text{Fe}]_{\text{dose}}$ ) in previous studies [23,27,35]. A recent study reported that the actual S/Fe molar ratio in the particles ( $[\text{S}/\text{Fe}]_{\text{particle}}$ ) via either co-sulfidation (using  $\text{Na}_2\text{S}_2\text{O}_4$ ) or post-sulfidation (using  $\text{Na}_2\text{S}$ ) was much lower than the relative  $[\text{S}/\text{Fe}]_{\text{dose}}$  [36], while another study reported that the  $[\text{S}/\text{Fe}]_{\text{particle}}$  of co-sulfidized S-nZVI (using  $\text{Na}_2\text{S}$ ) was close to the relative  $[\text{S}/\text{Fe}]_{\text{dose}}$  [37]. These results suggest that it is important to measure and report the  $[\text{S}/\text{Fe}]_{\text{particle}}$ , which would allow a better comparison between different studies and a better correlation between the sulfur content with their physicochemical properties. Moreover, these studies also indicate the impact of sulfur reagents on the actual sulfur content and reactivity of co-sulfidized S-nZVI. However, the impact of different sulfur reagents and their addition procedures on the sulfur content and speciation of post-sulfidized S-nZVI remains largely unknown.

Since water is the primary substance rather than the contaminants in water treatment, the inhibited side reaction between  $\text{Fe}^0$  and water by sulfidation is a more interesting property of S-nZVI from both the point of view of fundamental studies and applications. This would increase the S-nZVI longevity in water and improve the electron efficiency towards target contaminants [33,36,38]. Chlorinated contaminants have been widely used as reactivity probes to confirm the improved reactivity by the sulfidation of nZVI [27,33,34,37]. However, the defluorination of organics is much more difficult than dechlorination because C-F is more stable than C-Cl. It is unclear if sulfidation of nZVI will improve the reactivity for defluorination or if S-nZVI synthesized by different sulfidation methods and sulfur reagents will react differently for defluorination.

The existence and frequent occurrence of antibiotics would cause the emergence and dissemination of antibiotic resistant genes, and the degradation of antibiotics is of great importance to reduce antibiotic selection pressure of the environment [39]. As a frequent detected antibiotic, halogenated florfenicol (FF) was selected as the target contaminant in this study [40,41]. We synthesized S-nZVI via four different sulfidation methods, including a co-sulfidation method and three post-sulfidation methods with different sulfur reagents. This work aims to understand how sulfur reagents and sulfidation methods affect the morphology, chemical structure, and sulfur content-distribution-speciation of S-nZVI, and how these differences affect their reactivity with

water and FF. Density functional theory (DFT) calculations were performed to determine whether the amount and combination of S would affect the affinity of S-nZVI with water and H. Ultra performance liquid chromatography with tandem mass spectrometry (UPLC-MS/MS) analysis was performed to study the potential dehalogenation pathway of FF.

## 2. Experimental section

### 2.1. Materials

Analytical grade  $\text{FeCl}_3$ ,  $\text{NaBH}_4$ ,  $\text{Na}_2\text{S}_2\text{O}_4$ , HCl, NaOH, and  $\text{Na}_2\text{S}\cdot 9\text{H}_2\text{O}$  were obtained from Sinopharm Chemical Reagent Co., Ltd., China. High purity grade FF was obtained from Shanghai Ruichu Biotechnology Co., Ltd., China. Deschloro FF (one Cl atom on FF is replaced by one H atom) and dideschloro FF (two Cl atoms on FF are replaced by two H atoms) standard samples were obtained from Absin (Shanghai) Bioscience Inc., China. Ultrapure water was deoxygenated by purging nitrogen for 1 h before use.

### 2.2. Particles synthesis

nZVI and four S-nZVI particles were prepared according to previously reported methods [32,42–44]. Briefly, nZVI was synthesized by dropwise addition of 100 mL  $\text{NaBH}_4$  (0.51 g) solution into 175 mL  $\text{FeCl}_3$  (0.725 g) solution under stirring and nitrogen purging. Co-sulfidized S-nZVI (denoted as S-nZVI<sub>co</sub>) was synthesized by dropwise addition of 100 mL  $\text{NaBH}_4$  (0.51 g) and  $\text{Na}_2\text{S}_2\text{O}_4$  (0.054 g) mixed solution into 175 mL  $\text{FeCl}_3$  (0.725 g) solution, obtaining a theoretical  $[\text{S}/\text{Fe}]_{\text{dose}}$  of 0.14. For the other three post-sulfidation methods, 0.25 g nZVI was first synthesized, and washed three times by deoxygenated ultrapure water before dispersing into 100 mL water for the subsequent sulfidation. S-nZVI<sub>post-1</sub> was synthesized by mixing the nZVI suspension with 50 mL  $\text{Na}_2\text{S}_2\text{O}_4$  (0.054 g) solution, followed by ultrasonic treatment for 10 min, while S-nZVI<sub>post-2</sub> was obtained via the dropwise addition of 50 mL  $\text{Na}_2\text{S}_2\text{O}_4$  (0.054 g) solution into the nZVI suspension. S-nZVI<sub>post-3</sub> was synthesized by adding 50 mL  $\text{Na}_2\text{S}$  (0.049 g) solution into the nZVI suspension followed by ultrasonic treatment for 10 min. The targeted S/Fe molar ratio for each material were different, including 0.07, 0.14, 0.21, and 0.28  $[\text{S}/\text{Fe}]_{\text{dose}}$ , respectively. These materials were washed three times by deoxygenated ultrapure water and dried in a vacuum oven at 60 °C overnight, then the vacuum was filled by air and the materials were immediately taken out of the oven for reaction and characterizations.

### 2.3. Batch experiments

For the reactivity of nZVI or S-nZVI with water ( $\text{H}_2$  evolution), 50 mL 1.0 g L<sup>-1</sup> nZVI or different S-nZVI was added into 70 mL serum bottles, which were rotated on an end-over-end rotator (30 rpm) after immediately capped by Teflon Mininert valves. The  $\text{H}_2$  in the headspace (20 mL) was measured by a GC-TCD system at specific intervals. For the dechlorination reactivity (2 h) of nZVI and S-nZVI with FF, 0.28 mM FF was added into 500 mL three-necked flask containing 250 mL 1.0 g L<sup>-1</sup> nZVI or S-nZVI with continuously stirring (500 rpm) and nitrogen purging. For the defluorination reactivity (15 days) of nZVI or S-nZVI with FF removal, 0.28 mM FF was added into 70 mL serum bottles containing 50 mL 1.0 g L<sup>-1</sup> S-nZVI, which were rotated on an end-over-end rotator (30 rpm) after immediately capped by Teflon Mininert valves. Samples were taken out and immediately filtrated through 0.45 μm polyether sulfone membrane, the calibration curve after filtration was used to calculate FF concentrations in filtered samples.

### 2.4. Analytical methods

FF and dechlorinated products were quantified using high

performance liquid chromatography (HPLC, infinity 1260, Agilent, USA) equipped with UV-vis detector and a ZORBAX Eclipse XRD-C<sub>18</sub> column (250 × 4.6 mm, Agilent, USA). The mobile phase consisted of 40% methanol and 60% water at a flow rate of 1.0 mL min<sup>-1</sup>. Injection volume was 10 μL. The retention time of FF, deschloro FF, and dideschloro FF were 5.8, 4.1, and 3.2 min, respectively.

Ultra performance liquid chromatography with tandem mass spectrometry (UPLC-MS/MS, Waters, USA) equipped with a BEH C<sub>18</sub> column (2.1 × 100 mm, 1.7 μm, Waters, USA) was used to detect the defluorinated products of FF. Gradient eluted mobile phase was used with an initial ratio of water/methanol = 9/1 (v/v), water proportion decreased to 50% in the first 6 min and continuously declined to 5% in the following 2 min, then maintained for 1 min before increasing to 90% within 1 min. The entire testing time was 12 min including 2 min for washing the column and rebuilding the initial condition. The flow rate of mobile phase was 0.2 mL min<sup>-1</sup> and the injection volume was 4 μL.

The concentration of F<sup>-</sup> in the reactors was detected by ion chromatography (IC, Thermo Scientific ICS-5000), and a fluoride ion selective electrode was used to double-check the final F<sup>-</sup> concentration. The detection limit of the IC and fluoride ion selective electrode were 0.05 and 0.02 ppm, respectively. The actual [S/Fe]<sub>particle</sub> of each material was determined by inductively coupled plasma-optical emission spectrometry (ICP-OES) analysis after the digestion of a certain amount of S-nZVI particles in aqua regia [37].

TEM (FEI-Tecnaï G<sup>2</sup> F20), XRD (Rigaku-Ultima IV) and XPS (Thermo Scientific K-Alpha) were used to characterize the morphology, chemical structure and Fe and S species distribution, respectively. A pH meter (Mettler Toledo FE 20) and a portable multimeter (Hach HQ40d) were used to detect pH and ORP during the reaction, respectively.

### 2.5. Density functional theory (DFT) calculations

DFT calculations were conducted using the Vienna Ab initio Simulation Package. Electronic exchange and correlation were described by the generalized gradient approximation (GGA) method and the Perdew-Burke-Ernzerhof (PBE) functional [40]. The projector augmented-wave (PAW) method was used to describe the core electrons [41]. Valence electrons were described with the Kohn-Sham (KS) wave functions expanded in a plane wave basis with a kinetic energy cutoff of 400 eV [42]. The Brillouin zone was sampled with a (3 × 3 × 1) k-point mesh following the Monkhorst-Pack method [43]. Convergence was defined when the force on all atoms was lower than 0.05 eV Å<sup>-1</sup>. All calculations were conducted with spin-polarization. Fe(1 1 0) surfaces were modeled as four layer, (3 × 3) slabs. The choice to study the (1 1 0) is based upon our XRD measurements (Fig. 1f) showing that this is the predominant surface. Although Fe (hydro)oxides are inevitably existed on the surfaces of nZVI and S-nZVI particles, the surfaces covered with iron sulfides would be the most reactive surface than iron oxides. Hence, the impact of S combination with Fe on the hydrophobicity and the interaction with H was studied by DFT calculations. The S-in-Fe(1 1 0) surface was modeled with one surface Fe atom replaced with a S atom. The S-on-Fe(1 1 0) surface was modeled with the S atom adsorbed on the Fe(1 1 0) surface. For all calculations, the bottom two layers of the slabs were fixed, while the other two layers were relaxed. The hydrogen binding energy ( $E_b$ ) was calculated as:

$$E_b = E_{tot} - E_{surf} - \frac{1}{2}E_{H_2},$$

where  $E_{tot}$  is the total energy of the adsorption system,  $E_{surf}$  is the total energy of a bare surface, and  $E_{H_2}$  is the total energy of a H<sub>2</sub> molecule in vacuum.

## 3. Results and discussion

### 3.1. Characterizations

The morphology of pristine nZVI shows a typical chain-like structure that has been widely reported for nZVI [45–49], which consists of smooth and agglomerated spherical particles (Fig. 1a). Na<sub>2</sub>S<sub>2</sub>O<sub>4</sub> co-sulfidation and post-sulfidation particles exhibit ill-defined boundaries (Fig. 1b) and relatively more distinct spherical particles with irregular size (Fig. 1c and d), respectively. The Na<sub>2</sub>S post-sulfidation particles (Fig. 1e) show a similar structure as nZVI with an extra layer outside the particles, consistent with a previously reported Na<sub>2</sub>S post-sulfidized S-nZVI [50]. The particle size of S-nZVI<sub>post</sub> were calculated based on counting 130–150 particles (using the Image-Pro Plus software) from TEM images (Fig. 1c–e). S-nZVI<sub>post-1</sub> ([S/Fe]<sub>particle</sub> = 0.008) and S-nZVI<sub>post-2</sub> ([S/Fe]<sub>particle</sub> = 0.005) particles sulfidized by Na<sub>2</sub>S<sub>2</sub>O<sub>4</sub> were slightly larger than S-nZVI<sub>post-3</sub> ([S/Fe]<sub>particle</sub> = 0.003) sulfidized by Na<sub>2</sub>S. This increase in particles size was likely because iron sulfide phases coated onto the nZVI particles [51–54], and a higher sulfur content resulted in larger particles. These results indicate that both the sulfidation methods and sulfur reagents affected the morphology and size of S-nZVI.

Broad and small peaks of Fe<sup>0</sup> (Fe(1 1 0), Fe(2 0 0), and Fe(2 1 1)) were observed in the XRD spectra of nZVI and S-nZVI<sub>post</sub> particles (Fig. 1f). The peak position and intensity of nZVI and S-nZVI<sub>post</sub> were quite similar, suggesting that the post-sulfidation did not change much the crystal structure of nZVI. While for S-nZVI<sub>co</sub> particles, the intensity of Fe<sup>0</sup> peaks was much higher than that of nZVI and S-nZVI<sub>post</sub>, and all the Fe<sup>0</sup> peaks were shift to the left. This indicates that the co-sulfidation favors the generation of crystalline Fe<sup>0</sup> and sulfur is incorporated into the crystalline structure of Fe forming a solid-solution (alloy compound) rather than forming a phase-segregated structure or a physically-mixed structure [55,56]. The peaks for iron oxides and iron sulfides were not observed, suggesting that these phases were amorphous and/or present below the detection limit of XRD (~5 wt%).

The band gap of FeS, FeS<sub>2</sub>, Fe<sub>3</sub>S<sub>4</sub> is 0.10, 0.95, 0.00 eV, respectively, while the band gap of FeO, Fe<sub>2</sub>O<sub>3</sub>, Fe<sub>3</sub>O<sub>4</sub>, and FeOOH is 2.40, 2.20, 0.10, and 2.60 eV, respectively [57], indicating the faster electron transfer of iron sulfides than iron oxides. Herein, systematic XPS depth profiles (0, 10, 20, and 40 nm) of different S-nZVI were performed to not only show Fe and S species on the surface, but also give a general picture of the distribution of Fe and S species over the particles. As the sputtering depth increased (Fig. S1a), the Fe<sup>0</sup> intensity of S-nZVI<sub>co</sub> only slightly varied, and both the S and Fe were proved to be evenly distributed in our previous study [36]. In contrast, an uneven distribution of Fe<sup>0</sup> in S-nZVI<sub>post</sub> particles were observed (Fig. S1b–d), and the S/Fe atomic ratio according to the XPS analysis (Fig. S2a) shows a decreased trend as the analysis depth increased. These results indicate that there was more Fe<sup>0</sup> inside the particles and more S on the surface of S-nZVI<sub>post</sub>, which was consistent with TEM-EDX results of S-nZVI<sub>post</sub> as reported in a previous study [37]. During the co-sulfidation process, iron sulfides are likely formed along with the Fe<sup>0</sup> nucleation [58]. While for the post-sulfidation process, the surface reaction between the nZVI and sulfur reagents in the solution would be limited after forming a passivating FeS layer, thus sulfur would be present predominantly on the surface of S-nZVI<sub>post</sub> particles. [33,36].

The spatial speciation of sulfur was further studied (Fig. 2a–d), the peaks at 161.6, 162.6, 166.3, and 168.5 eV correspond to S<sup>2-</sup>, S<sub>2</sub><sup>2-</sup>, SO<sub>3</sub><sup>2-</sup> and SO<sub>4</sub><sup>2-</sup> respectively [59]. No oxidized sulfur species (SO<sub>3</sub><sup>2-</sup> and SO<sub>4</sub><sup>2-</sup>) were observed in the spectra of both surface and interior of S-nZVI<sub>co</sub> (Fig. 2a), indicating the improved anti-oxidation property of S-nZVI by co-sulfidation. For S-nZVI<sub>post-1</sub> (Fig. 2b) and S-nZVI<sub>post-3</sub> (Fig. 2d) with Na<sub>2</sub>S<sub>2</sub>O<sub>4</sub> or Na<sub>2</sub>S under ultrasonication, oxidized sulfur species (SO<sub>3</sub><sup>2-</sup> and SO<sub>4</sub><sup>2-</sup>) were observed on the surface but not found inside of the particles. While for S-nZVI<sub>post-2</sub> (Fig. 2c) with dropwise addition of Na<sub>2</sub>S<sub>2</sub>O<sub>4</sub>, SO<sub>3</sub><sup>2-</sup> species was observed at all depths



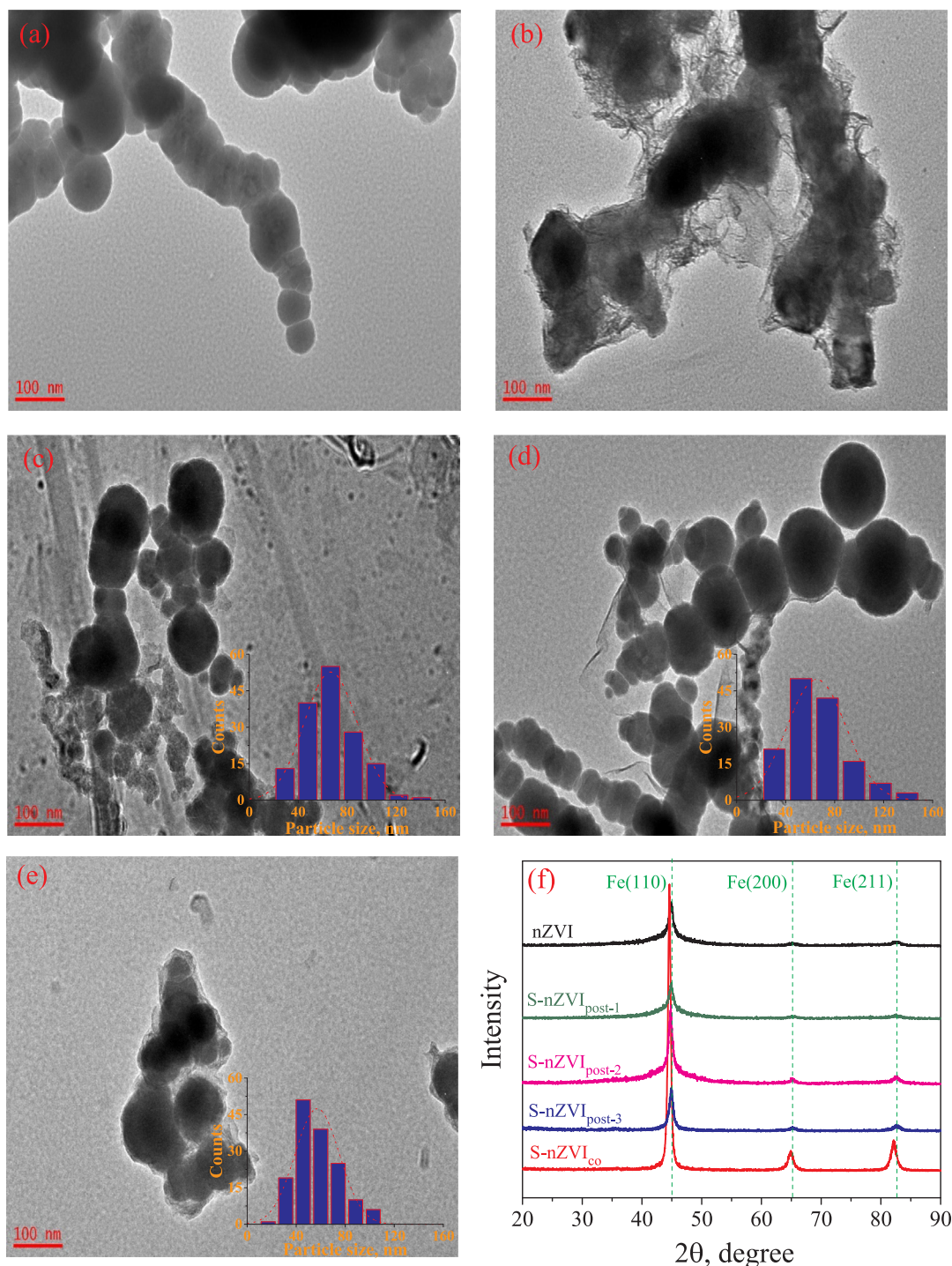


**Fig. 1.** TEM images of (a) nZVI, (b) S-nZVI<sub>co</sub>, (c) S-nZVI<sub>post-1</sub>, (d) S-nZVI<sub>post-2</sub>, and (e) S-nZVI<sub>post-3</sub> with their relative size distribution (counting 130–150 particles from TEM images); (f) XRD spectra of nZVI and different S-nZVI ([S/Fe]<sub>dose</sub> = 0.14).

investigated in this study. The fractions of the four sulfur species were counted by the relative normalized peak area (Fig. 2e–h). The sulfur distribution in S-nZVI shows similar trends with increasing depth: i) S<sup>2-</sup> and S<sub>2</sub><sup>2-</sup> species were observed in all of the S-nZVI samples at selected depths; ii) The fraction of S<sup>2-</sup> inside the particles was higher than that on the surface; iii) The content of oxidized sulfur species (SO<sub>3</sub><sup>2-</sup> and SO<sub>4</sub><sup>2-</sup>) in all the particles gradually decreased with increased depth.

The Fe<sup>0</sup> content of S-nZVI<sub>co</sub> sharply decreased when the [S/Fe]<sub>dose</sub> increased (Fig. 3a), indicating that the presence of Na<sub>2</sub>S<sub>2</sub>O<sub>4</sub> affected the reduction of Fe<sup>3+</sup> iron and increased the formation of iron sulfides. The [S/Fe]<sub>dose</sub> shows limited effects on the Fe<sup>0</sup> content of S-nZVI<sub>post</sub>. Since

the preparation conditions of S-nZVI vary in different labs, it is more important to measure and report the actual [S/Fe]<sub>particle</sub> rather than the [S/Fe]<sub>dose</sub>. The actual [S/Fe]<sub>particle</sub> of S-nZVI<sub>co</sub> gradually increased with the increase of [S/Fe]<sub>dose</sub> but was ~ 1.8–3.9 times lower than the [S/Fe]<sub>dose</sub> (Fig. 3b), indicating only partial incorporation of sulfur into the particles. The increased [S/Fe]<sub>particle</sub> was consistent with the decreased Fe<sup>0</sup> content in Fig. 3a. However, the [S/Fe]<sub>particle</sub> of S-nZVI<sub>post</sub> particles was significantly lower than the relative [S/Fe]<sub>dose</sub>, suggesting the very limited incorporation of sulfur into the nZVI by post-sulfidation methods, which was likely because the surface reaction between the sulfur reagent and nZVI in solution was limited by the formation of a

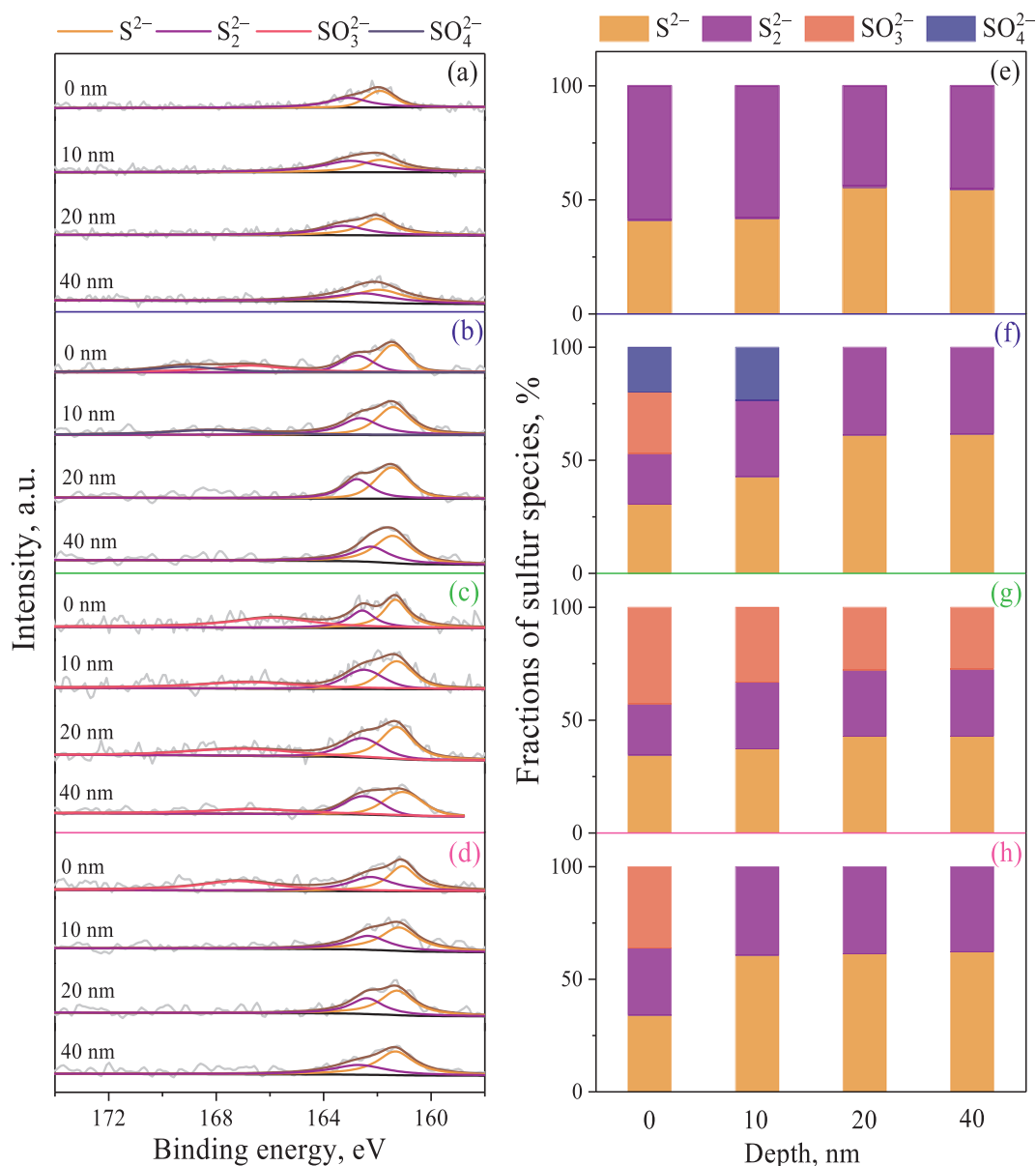


Fig. 2. S 2p XPS depth profiles and sulfur distribution of (a, e) S-nZVI<sub>co</sub>, (b, f) S-nZVI<sub>post-1</sub>, (c, g) S-nZVI<sub>post-2</sub>, and (d, h) S-nZVI<sub>post-3</sub> ([S/Fe]<sub>dose</sub> = 0.14).

passivating iron sulfide layer. Moreover, due to the higher sulfur content of S-nZVI<sub>post-1</sub> than S-nZVI<sub>post-3</sub>, it can be concluded that nZVI particles are more easily sulfidized by Na<sub>2</sub>S<sub>2</sub>O<sub>4</sub> than Na<sub>2</sub>S with the same sulfidation procedure. The significant differences of Fe<sup>0</sup> and sulfur content between co-sulfidation and post-sulfidation methods are important for their different reactivities and properties.

These characterization results show that the particles varied with different sulfidation methods, which affected the Fe crystalline structure, Fe<sup>0</sup> content, and sulfur content and spatial speciation. The co-sulfidation method incorporates more sulfur into the particles, resulting in more crystalline particles. The sulfur existed in a reduced state (S<sup>2-</sup> and S<sub>2</sub><sup>2-</sup>) rather than an oxidized state (SO<sub>3</sub><sup>2-</sup> and SO<sub>4</sub><sup>2-</sup>), but it also reduced the Fe<sup>0</sup> content. In contrast, the post-sulfidation methods did not incorporate much sulfur into the particles even at high doses and had little influence on the Fe<sup>0</sup> content. However, these post-sulfidation methods significantly affected the distribution of sulfur species both on the surface and inside the particles, which plays an important role in their reactivity as discussed later.

### 3.2. Suppressed water reactivity

The reactivity of S-nZVI with water was investigated via measurement of H<sub>2</sub> (Fe<sup>0</sup> + 2H<sub>2</sub>O → Fe<sup>2+</sup> + 2OH<sup>-</sup> + H<sub>2</sub>) over a 30 days period (Fig. S3), which was considered as a side reaction consuming the electrons from Fe<sup>0</sup>. In order to rule out the effect of surface area (Table S1) on the reactivity and to focus on the role of sulfur in the reactivity, the surface-area-normalized zero-order kinetics rate constants of H<sub>2</sub> evolution ( $k_{SA, H_2}$ ) were compared (Fig. 3c). The lowest  $k_{SA, H_2}$  by S-nZVI<sub>co</sub>, S-nZVI<sub>post-1</sub>, S-nZVI<sub>post-2</sub>, and S-nZVI<sub>post-3</sub> was ~31, 23, 11, and 16-fold lower than that by nZVI, respectively, suggesting that the reaction between Fe<sup>0</sup> and water was largely blocked, and that more electrons would go to reduce the contaminants. The  $k_{SA, H_2}$  by S-nZVI<sub>co</sub> gradually decreased with the increase of sulfur content. The very limited Fe<sup>0</sup> content (only 2% as shown in Fig. 3a) and high S content that could block the contact with H and water (as shown by our DFT modeling in Fig. 4), contributed to the negligible H<sub>2</sub> evolution at [S/Fe]<sub>dose</sub> = 0.28. This result indicates that the high sulfur content of S-nZVI via co-sulfidation would help to inhibit the side reaction with water, but it could also greatly reduce the Fe<sup>0</sup> content and capacity for

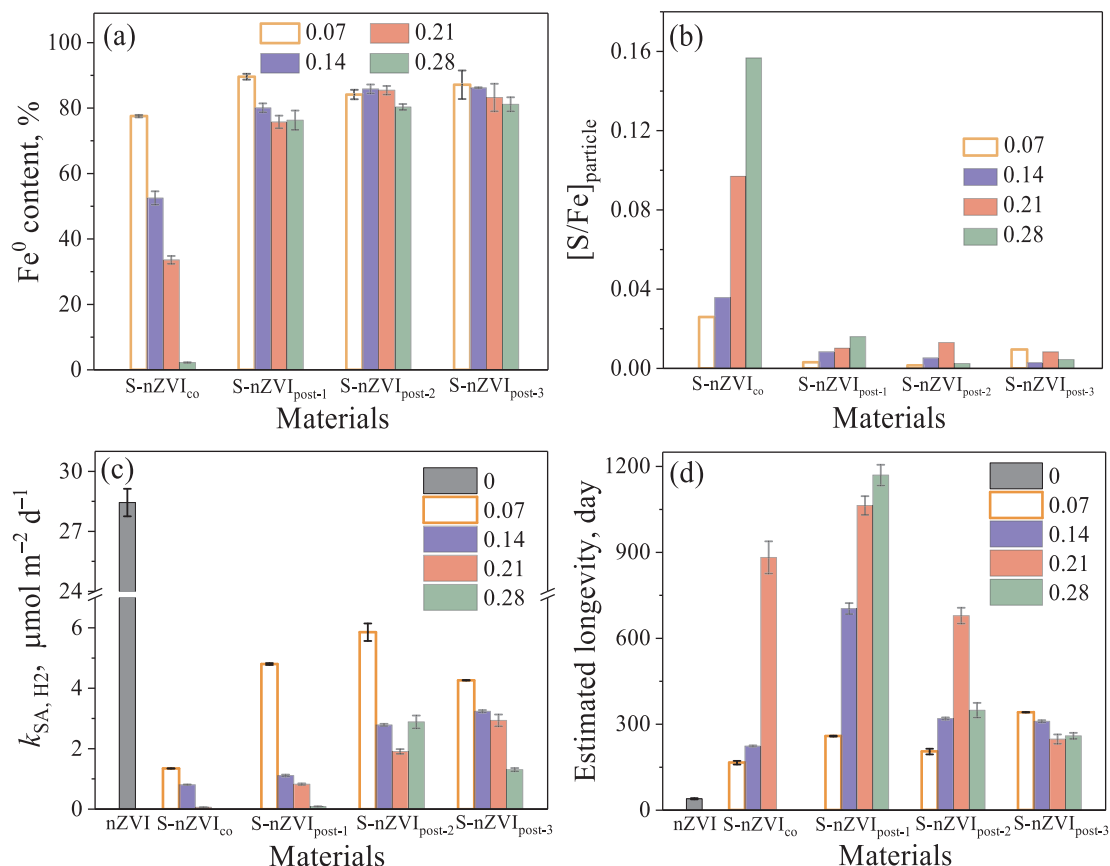


**Fig. 3.** (a)  $\text{Fe}^0$  content and (b) actual  $[\text{S}/\text{Fe}]_{\text{particle}}$  of S-nZVI via different sulfidation methods (the  $\text{Fe}^0$  content of nZVI was  $\sim 97\%$ ). (c)  $\text{H}_2$  evolution rate ( $k_{\text{SA}, \text{H}_2}$ ) and (d) estimated longevity in water ( $1.0 \text{ g L}^{-1}$  S-nZVI in water).

contaminants. Generally, the  $k_{\text{SA}, \text{H}_2}$  by S-nZVI<sub>post</sub> decreased at higher  $[\text{S}/\text{Fe}]_{\text{particle}}$  with the same sulfidation method.

The longevity of nZVI and S-nZVI was important for *in-situ* remediation, which would help to estimate the cost and how often to inject particles. The accumulated  $\text{H}_2$  based on the percentage of the actual  $\text{Fe}^0$  content of each material is shown in Fig. S3. The  $\text{H}_2$  evolution by S-nZVI followed zero-order kinetics (accumulated

$\text{H}_2 = k_{\text{obs}, \text{H}_2} \times t$ ). Hence, the longevity ( $t$ , day) of each material was estimated when the accumulated  $\text{H}_2$  (%) reached 100% (Fig. 3d). The  $\text{Fe}^0$  in nZVI was estimated to be exhausted after only  $\sim 40$  days in this study, while the longevity of S-nZVI<sub>co</sub>, S-nZVI<sub>post-1</sub>, S-nZVI<sub>post-2</sub>, and S-nZVI<sub>post-3</sub> was estimated to be up to 880, 1170, 680, and 340 days, respectively. The trends of  $k_{\text{SA}, \text{H}_2}$  and longevity correlated well with the actual  $[\text{S}/\text{Fe}]_{\text{particle}}$  (Fig. 3b) rather than  $[\text{S}/\text{Fe}]_{\text{dose}}$ , the higher

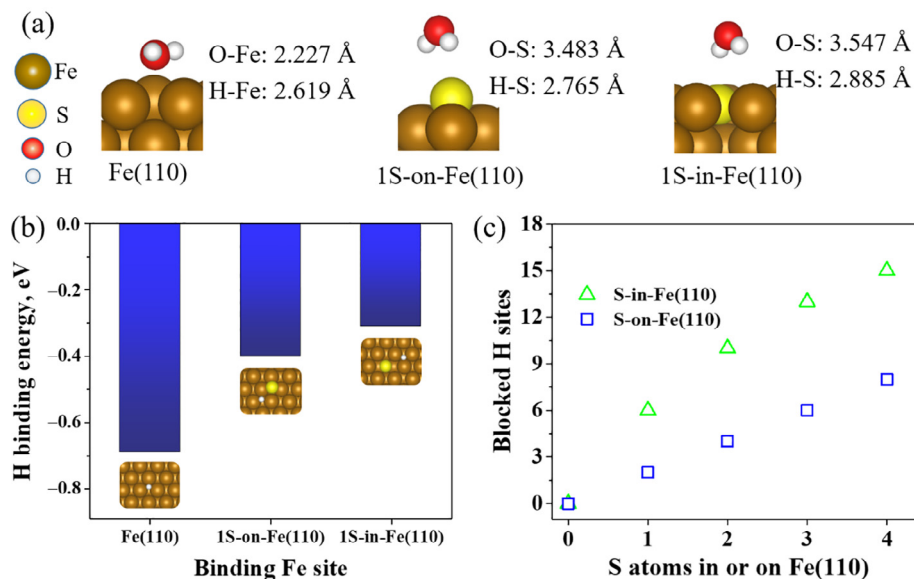


**Fig. 4.** (a) DFT-optimized adsorption geometries of water and (b) calculated H binding energies at Fe(1 1 0), 1S-on-Fe(1 1 0), and 1S-in-Fe(1 1 0) surfaces. Insets show the H adsorption geometries. (c) Number of blocked adsorption sites for H on Fe(1 1 0) surfaces with different modifications of S atoms.

actual  $[S/Fe]_{\text{particle}}$ , the lower  $k_{SA, H_2}$  and higher longevity. These correlations further emphasize the importance of measuring and reporting the actual  $[S/Fe]_{\text{particle}}$  of S-nZVI. Based on the comparison of the actual  $[S/Fe]_{\text{particle}}$  and  $k_{SA, H_2}$  of these three S-nZVI<sub>post</sub>, Na<sub>2</sub>S<sub>2</sub>O<sub>4</sub> sulfidation with ultrasonic was a more stable and controllable method, which shows a monotonously increasing trend of the actual  $[S/Fe]_{\text{particle}}$  (Fig. 3b), a monotonously decreasing trend of  $k_{SA, H_2}$  (Fig. 3c), and a monotonous increase in longevity (Fig. 3d).

It was previously reported that sulfur would block the adsorption sites for hydrogen [60–62], and sulfidation of nZVI would also make the particles more hydrophobic than nZVI [36]. However, any direct evidence for how the different S-Fe structures via different sulfidation methods affect these properties is limited. Herein, DFT calculations were performed to provide mechanistic insights into the role of sulfur in the material hydrophobicity and blocking of H adsorption sites. The XRD results indicated that the co-sulfidation method increased the crystallinity of Fe structure and sulfur was incorporated into the Fe crystalline structure, while post-sulfidation did not change the crystalline structure of Fe (Fig. 1f). Hence, to some extent, the models of Fe (1 1 0), S doped in Fe(1 1 0) (S-in-Fe(1 1 0)), and S bound on Fe(1 1 0) (S-on-Fe(1 1 0)) could potentially represent the Fe(1 1 0) surfaces of nZVI, co-sulfidized nZVI, and post-sulfidized nZVI, respectively. The affinities of water and hydrogen at these surfaces were evaluated by DFT calculations (Fig. 4).

Since the solvation effect is expected to have insignificant influence on the adsorption energetics under similar reaction environments [63,64], and due to the tremendous computational cost of spin-polarization and explicit solvation model in DFT, we did not consider an explicit solvation model in this study. The optimized adsorption geometries of water at Fe(1 1 0), 1S-on-Fe(1 1 0), and 1S-in-Fe(1 1 0) surfaces (Fig. 4a) clearly show that Fe(1 1 0) is a highly hydrophilic surface which stabilizes adsorption of water, while the S sites of both S-in-Fe(1 1 0) and S-on-Fe(1 1 0) are highly hydrophobic. In terms of hydrogen adsorption, it is found from the structural optimizations that a S atom can block 6 and 2 nearby adsorption sites for hydrogen on S-in-Fe(1 1 0) and S-on-Fe(1 1 0), respectively (Fig. 4c). Note that the blocked H sites on S-in-Fe(1 1 0) has been reported in our recent study [65], and is compared with S-on-Fe(1 1 0) here to show the effect of different S incorporations on the H adsorption. For the S-in-Fe(1 1 0) surface, hydrogen does not have stable adsorption geometries around the S site; instead, it migrates to the pure Fe<sub>3</sub> 3-fold hollow site nearby. This is attributed to the “ensemble effect”, where the hydrogen adsorption site is highly dependent on the specific arrangement and identity of surface atoms [66]. In contrast, the S atom in the S-on-Fe(1 1 0) surface blocks fewer potential H adsorption sites because it is the steric hindrance effect of S that blocks the adjacent adsorption site of H. The calculated H binding energies at the three surfaces show a clear trend in H adsorption energies (Fig. 4b), in the order of Fe(1 1 0) > S-on-Fe(1 1 0) > S-in-Fe(1 1 0). These results are in good agreement with the trends found from experiments that sulfidation of nZVI inhibited water dissociation as compared to nZVI without sulfidation. Using the number of blocked H sites on surface as a reactivity descriptor (Fig. 4c) it can be understood that compared to post-sulfidized nZVI, co-sulfidized S-nZVI, that incorporates S into the crystalline Fe structure, would in theory block more H adsorption sites. These calculations show that S-in-Fe(1 1 0) has less H affinity than S-on-Fe(1 1 0) due to both weaker H binding and more H site-blocking, consistent with a previous study that S-nZVI<sub>co</sub> was more hydrophobic than S-nZVI<sub>post</sub> based on the water contact angle measurements [36].

Both the experimental results (reaction with water) and the DFT calculations indicate that the sulfidation of nZVI inhibits contact between Fe<sup>0</sup> and water/H, and thus inhibits the H<sub>2</sub> evolution. Moreover, these properties suggest that sulfidation would also enhance the reactivity with hydrophobic contaminants (e.g. trichloroethene) or hydrophobic groups on contaminants (e.g. halogen groups) [30,34,67].

### 3.3. Enhanced dechlorination and defluorination

The FF removal by nZVI and S-nZVI with different sulfidation methods followed well with the pseudo-first order kinetics (Fig. S4), which was widely reported for the dechlorination of organic contaminants by nZVI and S-nZVI in previous studies [5,68–70]. The effect of sulfidation method on the dechlorination of FF by S-nZVI with the same  $[S/Fe]_{\text{dose}}$  (0.14) that characterized by XPS (known S species) was first compared (Fig. S5). The removal of FF by nZVI was significantly enhanced after sulfidation. S-nZVI<sub>co</sub> shows the highest reactivity with FF and the dechlorinated intermediate (deschloro FF) begin to decrease after 30 min (Fig. S5b), because the sulfur content (Fig. 3b) and surface area (Table S1) of S-nZVI<sub>co</sub> was higher than the other three S-nZVI<sub>post</sub>, and all the sulfur was in the form of sulfide (S<sub>2</sub><sup>2-</sup>) and disulfide (S<sub>2</sub><sup>2-</sup>) (Fig. 2e) with relatively lower band gap than iron oxides [57]. The higher content of sulfur would facilitate the electron transfer to the contaminant but block the adsorption of H and provide more hydrophobic sites (Fig. 4). The dechlorination of FF by S-nZVI<sub>post-3</sub> was slightly faster than that by S-nZVI<sub>post-1</sub>. Although the surface area (Table S1) and actual sulfur content (Fig. 3b) of S-nZVI<sub>post-3</sub> were lower than that of S-nZVI<sub>post-1</sub>, most of the sulfur in S-nZVI<sub>post-3</sub> was mainly in the form of S<sub>2</sub><sup>2-</sup> and S<sub>2</sub><sup>2-</sup> with few SO<sub>3</sub><sup>2-</sup> on the surface, while there was more oxidized sulfur species (SO<sub>3</sub><sup>2-</sup> and SO<sub>4</sub><sup>2-</sup>) existed on the surface of S-nZVI<sub>post-1</sub> (Fig. 2f). The lowest rate of FF dechlorination by S-nZVI<sub>post-2</sub> was also consistent with its low sulfur content and the highest SO<sub>3</sub><sup>2-</sup> species content (Fig. 2g). These results suggested that both the sulfur content and species played important roles in the reactivity of S-nZVI. ORP is a measurement of the electron activity in the solution and indicates the relative tendency to transfer or accept electrons [71]. The ORP of these S-nZVI suspension during the reaction (Fig. S5e) also consistent with the trend of reactivity, the lower ORP, the higher reactivity, suggesting the ORP might be a simple indicator for the comparison of the reactivity of S-nZVI synthesized via different sulfidation methods. The pH of different S-nZVI systems dropped in the first 20 min then became stable during the reaction (Fig. S5f), and there was no significant difference between different S-nZVI systems.

The effects of sulfur reagents and sulfidation methods on the FF removal by S-nZVI are shown in Figs. S6–9, and the relative surface-area-normalized rates of FF removal ( $k_{SA, FF}$ ) were calculated (Fig. 5a). The removal rate of FF by S-nZVI<sub>co</sub> was increased when the  $[S/Fe]_{\text{particle}}$  increased from 0.026 to 0.097, while obviously decreased when the  $[S/Fe]_{\text{particle}}$  further increased to 0.157 because of the limited Fe<sup>0</sup> content (~2%). This indicates that both the sulfur amount and Fe<sup>0</sup> content could affect the dechlorination of FF. The FF removal by S-nZVI<sub>post-1</sub> (Fig. 5a) was also positively correlated with the sulfur content (Fig. 3b). Since the actual  $[S/Fe]_{\text{particle}}$  of S-nZVI<sub>post-2</sub> and S-nZVI<sub>post-3</sub> particles was similar, the decreased trend of  $k_{SA, FF}$  was possibly attributed to the changes of morphology, sulfur species, and electron transfer ability, which were interesting ongoing studies to explore the sulfur chemistry involved in the environmental remediation by S-nZVI.

The dechlorination of FF (Fig. S10) was much faster than the defluorination (Fig. S11), 100% of FF was dechlorinated within 3 days (according to the measurement of Cl<sup>-</sup> in the solution) for all the particles except the S-nZVI<sub>co</sub> with a low Fe<sup>0</sup> content (~2%) (Fig. 5b and S10). The defluorination of FF by S-nZVI with different sulfidation methods were explored based on the F<sup>-</sup> generation over a 15 days reaction (Fig. S11). Almost no F<sup>-</sup> was detected after 2 h reaction of FF with nZVI (Fig. 5c), while about 2–6% of 100 mg L<sup>-1</sup> FF was defluorinated (1–3 mg L<sup>-1</sup> FF per hour) by S-nZVI, which are comparable with a recently reported defluorination of FF (~2 mg L<sup>-1</sup> FF per hour) by a CoP/Ti electrode [72]. Although the defluorination performance will be varied with experimental conditions (e.g. materials dose, applied potential), these two methods will be potential technologies for the defluorination of FF in different scenarios (e.g. *in-situ* or *ex-situ*, respectively). The initial (first 2 h) defluorination efficiency of FF by different S-nZVI was correlated well with their relative  $[S/Fe]_{\text{particle}}$



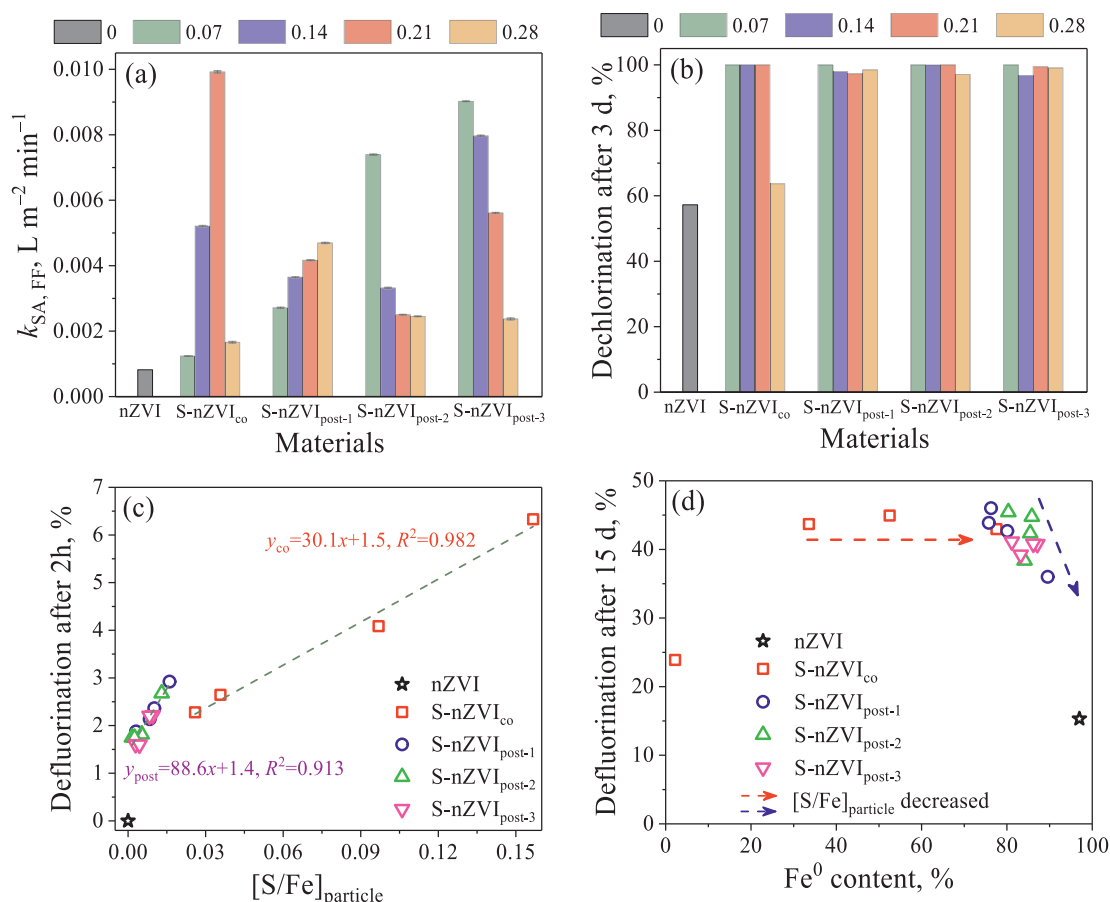


Fig. 5. (a) Pseudo-first-order rate constant of FF removal by nZVI and S-nZVI with different  $[S/Fe]_{\text{dose}}$  within 2 h reaction; (b) dechlorination of FF removal after 1 d reaction; (c) correlation of initial (2 h reaction) defluorination with  $[S/Fe]_{\text{particle}}$ ; (d) correlation of long-term (15 d reaction) defluorination with  $Fe^0$  content (basic conditions:  $T = 25\text{ }^{\circ}\text{C}$ , initial  $\text{pH} = 7.0$ ,  $0.28\text{ mM FF}$ ,  $1.0\text{ g L}^{-1}$  nZVI or S-nZVI).

(Fig. 5c), that is, higher  $[S/Fe]_{\text{particle}}$  achieved higher defluorination of FF, which further confirmed the importance of measuring and reporting the actual  $[S/Fe]_{\text{particle}}$ . The fitted linear slopes of defluorination of FF by S-nZVI<sub>co</sub> and S-nZVI<sub>post</sub> were obviously different, and some S-nZVI<sub>post</sub> with lower  $[S/Fe]_{\text{particle}}$  could defluorinate more FF than co-sulfidized S-nZVI, despite the S contents in S-nZVI<sub>post</sub> were  $\sim 3\text{--}60$  times lower than those in S-nZVI<sub>co</sub> (Fig. 3b). Moreover, the surface S/Fe molar ratios of S-nZVI<sub>post</sub> were higher than that of S-nZVI<sub>co</sub> (Fig. S2b), and there were more reduced S forms (e.g. FeS and FeS<sub>2</sub>) on the surface of S-nZVI<sub>post</sub> than those on the surface of S-nZVI<sub>co</sub> (Fig. S2c), which were expected to improve the reactivity [73]. The oxidative S forms (e.g. SO<sub>3</sub><sup>2-</sup> and SO<sub>4</sub><sup>2-</sup>) would not favor the reactivity [74]. These results indicate that the sulfur in S-nZVI<sub>post</sub> was more available for the reaction with FF because there was more sulfur on the surface of S-nZVI<sub>post</sub> than S-nZVI<sub>co</sub>. However, the S-nZVI<sub>co</sub> material with higher  $[S/Fe]_{\text{particle}}$  (0.157) but limited  $Fe^0$  ( $\sim 2\%$ ) content only defluorinated  $\sim 25\%$  of FF after 15 days reaction, while other S-nZVI materials could achieve 40–50% of defluorination (Fig. S11). Note that the defluorination of FF by S-nZVI<sub>co</sub> using  $Fe^{2+}$  precursor ( $\sim 30\%$  after 4 months) in our previous study [26] was much slower than that by S-nZVI<sub>co</sub> using  $Fe^{3+}$  precursor in this study (Fig. S12) under the same experimental conditions (dose, pH, temperature, etc.), the reasons for this phenomenon are unclear, it is anticipated that the crystal structure, electron transfer, hydrophobicity, sulfur content and speciation are all possible reasons. The  $Fe^0$  content became another factor for the long-term defluorination of FF by S-nZVI, especially for S-nZVI<sub>co</sub> with 2%  $Fe^0$  content, which clearly became less reactive for defluorination (Fig. 5d). While for the S-nZVI<sub>post</sub> particles with similar  $Fe^0$  content, and the defluorination of FF was slightly decreased with the decreased sulfur content. These results

suggest that both the  $Fe^0$  content and sulfur content would affect the defluorination of FF by S-nZVI materials.

### 3.4. Reaction mechanism

Four dechlorination and defluorination products of FF removal by S-nZVI were detected by UPLC-MS/MS, including deschloro FF (C<sub>12</sub>H<sub>15</sub>O<sub>4</sub>NSClF), dideschloro FF (C<sub>12</sub>H<sub>16</sub>O<sub>4</sub>NSF), product-287 (C<sub>12</sub>H<sub>17</sub>O<sub>5</sub>NS), and product-269 (C<sub>12</sub>H<sub>15</sub>O<sub>4</sub>NS) (Figs. S13–16). This result suggests that the sulfidation method and sulfur content of S-nZVI did not affect the degradation pathway of FF. The mass signal of dechlorinated product-289 (dideschloro FF) (Fig. 6a) and defluorinated product-269 (Fig. 6b) was increased during the first 3 days reaction and then gradually decreased afterwards, while product-287 (Fig. 6c) was continuously accumulated throughout the entire reaction time (15 days).

Proposed dechlorination and defluorination pathway of FF by S-nZVI was illustrated in Fig. 6d. The dechlorination of FF was prior to and much faster than the defluorination of FF by S-nZVI. The chlorine in FF molecule was removed one by one through hydrogenolysis, which was indicated by the same generation rate of dideschloro FF before and after all the parent FF was gone (Figs. S6–9). Dideschloro FF could be defluorinated to product-269 through the  $\beta$ -elimination reaction and followed by the addition reaction to form product-287. It was also possible that dideschloro FF could be defluorinated to product-287 via substitution. The decreased trend of product-269 after 3 days (Fig. 6b) was likely due to the addition of C=C bond with water, transforming to product-287. The performance of S-nZVI for defluorination at room temperature and pressure endows S-nZVI with a new property that is



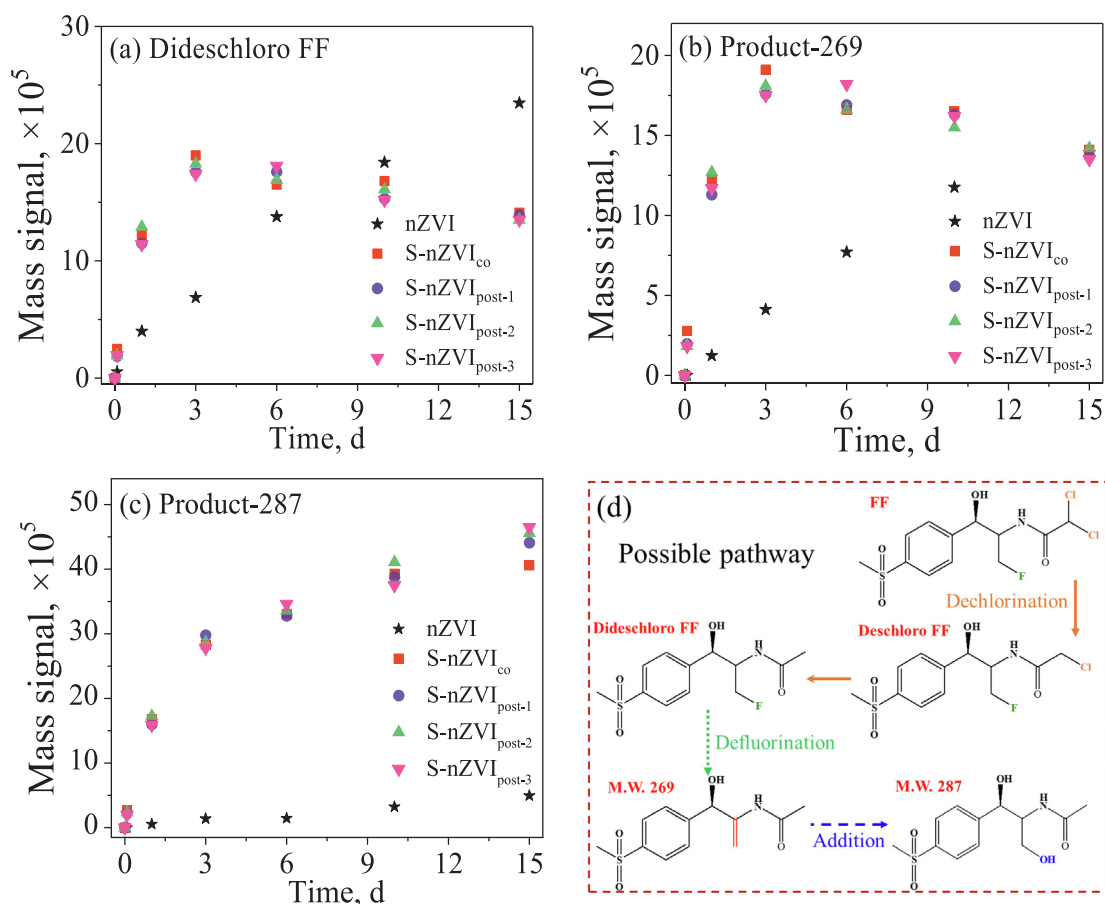


Fig. 6. Mass signal changes of (a) dideschloro FF, (b) product-269 and (c) product-287 during the reaction. (d) Proposed degradation pathway of FF by S-nZVI ( $T = 25\text{ }^{\circ}\text{C}$ , initial  $\text{pH} = 7.0$ ,  $0.28\text{ mM FF}$ ,  $1.0\text{ g L}^{-1}$  S-nZVI with  $0.14\text{ [S/Fe]}_{\text{dose}}$ ).

unexpected before.

#### 4. Conclusions

These results suggest that both the sulfidation method and sulfur reagents can influence the Fe crystalline structure,  $\text{Fe}^0$  content, and sulfur content and spatial speciation, which further affect their reactivity with water and halogenated contaminants. These influences also suggest the importance of regarding the sulfidation method and sulfur content for comparisons of S-nZVI in literatures. Sulfur not only acts as a hydrophobic site to inhibit the contact between water and the material, but also blocks the adsorption sites for H, reducing reduces the reactivity of S-nZVI with water and extending extends the reactive lifetime in water. Compared to post-sulfidation methods, the co-sulfidation method promotes the formation of crystalline  $\text{Fe}^0$  structure, incorporates more sulfur into the particles, and maintains the sulfur in the forms of  $\text{S}^{2-}$  and  $\text{S}_2^{2-}$  species rather than in oxidized sulfur forms (e.g.  $\text{SO}_3^{2-}$  and  $\text{SO}_4^{2-}$ ). The sulfur content controls the initial reactivity for defluorination, and the  $\text{Fe}^0$  content became another important factor for the long-term performance.

The sulfidation method and sulfur content did not change the degradation pathway, though the dechlorination and defluorination rates of FF by different S-nZVI were different due to their unique structure,  $\text{Fe}^0$  content, and sulfur content. FF could be possibly removed through hydrogenolysis, substitution,  $\beta$ -elimination, and addition reactions by all kinds of S-nZVI according to the UPLC-MS/MS analysis. But further efforts are needed to figure out the precise role of sulfur in these reactions, especially for defluorination. S-nZVI can be a potential technology for defluorination at room temperature and pressure. Besides, polymeric surface modification is encouraged to deliver the S-nZVI

particles to subsurface remediation and to study the effects of dissolved groundwater solutes on the performance [74,75].

S-nZVI particles with high reactivity with contaminant but limited reactivity with water would not only shorten the remediation period but also greatly reduce the cost, and these S-nZVI with different sulfidation methods and sulfur content would be alternatives for different application scenarios. A better understanding on the role of sulfur in the physicochemical properties and reactivity of different S-nZVI forms will also pave for the rational design of S-nZVI in the future.

#### Declaration of interests

The authors declare that they have no known competing financial interests or personal relationships that could have appeared to influence the work reported in this paper.

#### Acknowledgements

The authors thank Dr. Gregory Lowry for providing the instruments and lab space for measuring the  $\text{Fe}^0$  content and  $\text{H}_2$ . The authors would like to acknowledge the National Natural Science Foundation of China (No. 41877463) for financial support. The calculations were supported by the Texas Advanced Computing Center and the Welch Foundation (F-1841).

#### Appendix A. Supplementary data

Supplementary data to this article can be found online at <https://doi.org/10.1016/j.cej.2020.125900>.

## References

- [1] A. Wei, J. Ma, J. Chen, Y. Zhang, J. Song, X. Yu, Enhanced nitrate removal and high selectivity towards dinitrogen for groundwater remediation using biochar-supported nano zero-valent iron, *Chem. Eng. J.* 353 (2018) 595–605.
- [2] M. Gu, Q. Sui, U. Farooq, X. Zhang, Z. Qiu, S. Lyu, Enhanced degradation of trichloroethylene in oxidative environment by nZVI/PDA functionalized rGO catalyst, *J. Hazard. Mater.* 359 (2018) 157–165.
- [3] S. Zhang, M. Wu, T. Tang, Q. King, C. Peng, F. Li, H. Liu, X. Luo, J. Zou, X. Min, J. Luo, Mechanism investigation of anoxic Cr(VI) removal by nano zero-valent iron based on XPS analysis in time scale, *Chem. Eng. J.* 335 (2018) 945–953.
- [4] J. Xu, Z. Hao, C. Xie, X. Lv, Y. Yang, X. Xu, Promotion effect of Fe<sup>2+</sup> and Fe<sub>3</sub>O<sub>4</sub> on nitrate reduction using zero-valent iron, *Desalination* 284 (2012) 9–13.
- [5] X. Liu, Z. Cao, Z. Yuan, J. Zhang, X. Guo, Y. Yang, F. He, Y. Zhao, J. Xu, Insight into the kinetics and mechanism of removal of aqueous chlorinated nitroaromatic antibiotic chloramphenicol by nanoscale zero-valent iron, *Chem. Eng. J.* 334 (2018) 508–518.
- [6] J. Xu, Z. Cao, X. Liu, H. Zhao, X. Xiao, J. Wu, X. Xu, J.L. Zhou, Preparation of functionalized Pd/Fe-Fe<sub>3</sub>O<sub>4</sub>@MWCNTs nanomaterials for aqueous 2, 4-dichlorophenol removal: interactions, influence factors, and kinetics, *J. Hazard. Mater.* 317 (2016) 656–666.
- [7] B.D. Yirsaw, M. Megharaj, Z. Chen, R. Naidu, Environmental application and ecological significance of nano-zero valent iron, *J. Environ. Sci.* 44 (2016) 88–98.
- [8] Y. Zou, X. Wang, A. Khan, P. Wang, Y. Liu, A. Alsaedi, T. Hayat, X. Wang, Environmental remediation and application of nanoscale zero-valent iron and its composites for the removal of heavy metal ions: a review, *Environ. Sci. Technol.* 50 (2016) 7290–7304.
- [9] T. Phenrat, G.V. Lowry, Nanoscale Zerovalent Iron Particles for Environmental Restoration: From Fundamental Science to Field Scale Engineering Applications, Springer International Publishing, 2019.
- [10] S. Bhattacharjee, M. Basnet, N. Tufenkji, S. Ghoshal, Effects of rhamnolipid and carboxymethylcellulose coatings on reactivity of palladium-doped nanoscale zero-valent iron particles, *Environ. Sci. Technol.* 50 (2016) 1812–1820.
- [11] M. Cohen, N. Weisbrod, Field scale mobility and transport manipulation of carbon-supported nanoscale zero-valent iron (nZVI) in fractured media, *Environ. Sci. Technol.* 52 (2018) 7849–7858.
- [12] Y. Wu, Q. Yue, Z. Ren, B. Gao, Immobilization of nanoscale zero-valent iron particles (nZVI) with synthesized activated carbon for the adsorption and degradation of Chloramphenicol (CAP), *J. Mol. Liq.* 262 (2018) 19–28.
- [13] T. Phenrat, N. Saleh, K. Sirk, R.D. Tilton, G.V. Lowry, Aggregation and sedimentation of aqueous nanoscale zerovalent iron dispersions, *Environ. Sci. Technol.* 41 (2007) 284–290.
- [14] S. Wu, M. Vosátka, K. Vogel-Mikus, A. Kavčič, M. Kelemen, L. Šepec, P. Pelicon, R. Skála, A.R. Valero Powter, M. Teodoro, Z. Michálková, M. Komárek, Nano zero-valent iron mediated metal(loid) uptake and translocation by arbuscular mycorrhizal symbioses, *Environ. Sci. Technol.* 52 (2018) 7640–7651.
- [15] T. Shubair, O. Eljamal, A.M.E. Khalil, A. Tahara, N. Matsunaga, Novel application of nanoscale zero valent iron and bimetallic nano-Fe/Cu particles for the treatment of cesium contaminated water, *J. Environ. Chem. Eng.* 6 (2018) 4253–4264.
- [16] J. Xu, J. Tang, S.A. Baig, X. Lv, X. Xu, Enhanced dechlorination of 2, 4-dichlorophenol by Pd/Fe-Fe<sub>3</sub>O<sub>4</sub> nanocomposites, *J. Hazard. Mater.* 244–245 (2013) 628–636.
- [17] J. Xu, L. Tan, S.A. Baig, D. Wu, X. Lv, X. Xu, Dechlorination of 2, 4-dichlorophenol by nanoscale magnetic Pd/Fe particles: effects of pH, temperature, common dissolved ions and humic acid, *Chem. Eng. J.* 231 (2013) 26–35.
- [18] S. Zhu, S. Ho, X. Huang, D. Wang, F. Yang, L. Wang, C. Wang, X. Cao, F. Ma, Magnetic nanoscale zerovalent iron assisted biochar: interfacial chemical behaviors and heavy metals remediation performance, *ACS Sustain. Chem. Eng.* 5 (2017) 9673–9682.
- [19] X. Jiang, Z. Ouyang, Z. Zhang, C. Yang, X. Li, Z. Dang, P. Wu, Mechanism of glyphosate removal by biochar supported nano-zero-valent iron in aqueous solutions, *Colloid Surf. A* 547 (2018) 64–72.
- [20] P.K. Mondal, P.D. Furbacher, Z. Cui, M.M. Krol, B.E. Sleep, Transport of polymer stabilized nano-scale zero-valent iron in porous media, *J. Contam. Hydrol.* 212 (2018) 65–77.
- [21] J. Xu, T. Sheng, Y. Hu, S.A. Baig, X. Lv, X. Xu, Adsorption-dechlorination of 2, 4-dichlorophenol using two specified MWCNTs-stabilized Pd/Fe nanocomposites, *Chem. Eng. J.* 219 (2013) 162–173.
- [22] J. Xu, X. Liu, G.V. Lowry, Z. Cao, H. Zhao, J.L. Zhou, X. Xu, Dechlorination mechanism of 2, 4-dichlorophenol by magnetic MWCNTs supported Pd/Fe nanohybrids: Rapid adsorption, gradual dechlorination, and desorption of phenol, *ACS Appl. Mater. Inter.* 8 (2016) 7333–7342.
- [23] Y. Su, A.S. Adeleye, A.A. Keller, Y. Huang, C. Dai, X. Zhou, Y. Zhang, Magnetic sulfide-modified nanoscale zerovalent iron (S-nZVI) for dissolved metal ion removal, *Water Res.* 74 (2015) 47–57.
- [24] C. Xu, B. Zhang, Y. Wang, Q. Shao, W. Zhou, D. Fan, J.Z. Bandstra, Z. Shi, P.G. Tratnyek, Effects of sulfidation, magnetization, and oxygenation on azo dye reduction by zerovalent iron, *Environ. Sci. Technol.* 50 (2016) 11879–11887.
- [25] D. Wu, S. Peng, K. Yan, B. Shao, Y. Feng, Y. Zhang, Enhanced As(III) sequestration using sulfide-modified nano-scale zero-valent iron with a characteristic core-shell structure: sulfidation and As distribution, *ACS Sustain. Chem. Eng.* 6 (2018) 3039–3048.
- [26] J. Xu, Z. Cao, Y. Wang, Y. Zhang, X. Gao, M.B. Ahmed, J. Zhang, Y. Yang, J.L. Zhou, G.V. Lowry, Distributing sulfidized nanoscale zerovalent iron onto phosphorus-functionalized biochar for enhanced removal of antibiotic florfenicol, *Chem. Eng. J.* 359 (2019) 713–722.
- [27] H. Dong, C. Zhang, J. Deng, Z. Jiang, L. Zhang, Y. Cheng, K. Hou, L. Tang, G. Zeng, Factors influencing degradation of trichloroethylene by sulfide-modified nanoscale zero-valent iron in aqueous solution, *Water Res.* 135 (2018) 1–10.
- [28] Z. Cao, X. Liu, J. Xu, J. Zhang, Y. Yang, J. Zhou, X. Xu, G.V. Lowry, Removal of antibiotic florfenicol by sulfide-modified nanoscale zero-valent iron, *Environ. Sci. Technol.* 51 (2017) 11269–11277.
- [29] S. Song, Y. Su, A.S. Adeleye, Y. Zhang, X. Zhou, Optimal design and characterization of sulfide-modified nanoscale zerovalent iron for diclofenac removal, *Appl. Catal. B* 201 (2017) 211–220.
- [30] D. Li, Z. Mao, Y. Zhong, W. Huang, Y. Wu, P.A. Peng, Reductive transformation of tetrabromobisphenol A by sulfidated nano zerovalent iron, *Water Res.* 103 (2016) 1–9.
- [31] Y. Su, D. Jassby, S. Song, X. Zhou, H. Zhao, J. Filip, E. Petala, Y. Zhang, Enhanced oxidative and adsorptive removal of diclofenac in heterogeneous fenton-like reaction with sulfide modified nanoscale zerovalent iron, *Environ. Sci. Technol.* 52 (2018) 6466–6475.
- [32] E.J. Kim, J.H. Kim, A.M. Azad, Y.S. Chang, Facile synthesis and characterization of Fe/FeS nanoparticles for environmental applications, *ACS Appl. Mater. Inter.* 3 (2011) 1457–1462.
- [33] S.R.C. Rajajayavel, S. Ghoshal, Enhanced reductive dechlorination of trichloroethylene by sulfidated nanoscale zerovalent iron, *Water Res.* 78 (2015) 144–153.
- [34] Y. Han, W. Yan, Reductive dechlorination of trichloroethene by zero-valent iron nanoparticles: reactivity enhancement through sulfidation treatment, *Environ. Sci. Technol.* 50 (2016) 12992–13001.
- [35] J. Li, X. Zhang, M. Liu, B. Pan, W. Zhang, Z. Shi, X. Guan, Enhanced reactivity and electron selectivity of sulfidated zerovalent iron toward chromate under aerobic conditions, *Environ. Sci. Technol.* 52 (2018) 2988–2997.
- [36] J. Xu, Y. Wang, C. Weng, W. Bai, Y. Jiao, R. Kaegi, G.V. Lowry, Reactivity, selectivity, and long-term performance of sulfidized nanoscale zerovalent iron with different properties, *Environ. Sci. Technol.* 53 (2019) 5936–5945.
- [37] S. Bhattacharjee, S. Ghoshal, Optimal design of sulfidated nanoscale zerovalent iron for enhanced trichloroethene degradation, *Environ. Sci. Technol.* 52 (2018) 11078–11086.
- [38] D. Fan, G.O. Brien Johnson, P.G. Tratnyek, R.L. Johnson, Sulfidation of nano zero-valent iron (nZVI) for improved selectivity during in-situ chemical reduction (ISCR), *Environ. Sci. Technol.* 50 (2016) 9558–9565.
- [39] X. Guo, Y. Yang, D. Lu, Z. Niu, J. Feng, Y. Chen, F. Tou, E. Garner, J. Xu, M. Liu, M.F. Hochella, Biofilms as a sink for antibiotic resistance genes (ARGs) in the Yangtze Estuary, *Water Res.* 129 (2018) 277–286.
- [40] F.C. Cabello, H.P. Godfrey, A. Tomova, L. Ivanova, H. Dölz, A. Millanao, A.H. Buschmann, Antimicrobial use in aquaculture re-examined: its relevance to antimicrobial resistance and to animal and human health, *Environ. Microbiol.* 15 (2013) 1917–1942.
- [41] H. Zhao, Z. Cao, X. Liu, Y. Zhan, J. Zhang, X. Xiao, Y. Yang, J.L. Zhou, J. Xu, Seasonal variation, flux estimation, and source analysis of dissolved emerging organic contaminants in the Yangtze Estuary, China, *Mar. Pollut. Bull.* 125 (2017) 208–215.
- [42] C. Wang, W. Zhang, Synthesizing Nanoscale iron particles for rapid and complete dechlorination of TCE and PCBs, *Environ. Sci. Technol.* 31 (1997) 2154–2156.
- [43] Y. Xie, D.M. Cwiertny, Use of dithionite to extend the reactive lifetime of nanoscale zero-valent iron treatment systems, *Environ. Sci. Technol.* 44 (2010) 8649–8655.
- [44] J. Tang, L. Tang, H. Feng, G. Zeng, H. Dong, C. Zhang, B. Huang, Y. Deng, J. Wang, Y. Zhou, pH-dependent degradation of p-nitrophenol by sulfidated nanoscale zerovalent iron under aerobic or anoxic conditions, *J. Hazard. Mater.* 320 (2016) 581–590.
- [45] Y. Hwang, D. Kim, H. Shin, Mechanism study of nitrate reduction by nano zero valent iron, *J. Hazard. Mater.* 185 (2011) 1513–1521.
- [46] H.K. Boparai, M. Joseph, D.M.O. Carroll, Kinetics and thermodynamics of cadmium ion removal by adsorption onto nano zerovalent iron particles, *J. Hazard. Mater.* 186 (2011) 458–465.
- [47] X. Wang, P. Wang, J. Ma, H. Liu, P. Ning, Synthesis, characterization, and reactivity of cellulose modified nano zero-valent iron for dye discoloration, *Appl. Surf. Sci.* 345 (2015) 57–66.
- [48] Y. Hwang, D. Kim, H. Shin, Effects of synthesis conditions on the characteristics and reactivity of nano scale zero valent iron, *Appl. Catal. B* 105 (2011) 144–150.
- [49] D. Lv, J. Zhou, Z. Cao, J. Xu, Y. Liu, Y. Li, K. Yang, Z. Lou, L. Lou, X. Xu, Mechanism and influence factors of chromium(VI) removal by sulfide-modified nanoscale zero-valent iron, *Chemosphere* 224 (2019) 306–315.
- [50] J. Xu, Z. Cao, H. Zhou, Z. Lou, Y. Wang, X. Xu, G.V. Lowry, Sulfur dose and sulfidation time affect reactivity and selectivity of post-sulfidated nanoscale zerovalent iron, *Environ. Sci. Technol.* 53 (2019) 13344–13352.
- [51] Q. Zhang, W. Guo, X. Yue, Z. Liu, X. Li, Degradation of rhodamine B using FeS-coated zero-valent iron nanoparticles in the presence of dissolved oxygen, *Environ. Prog. Sustain.* 35 (2016) 1673–1678.
- [52] E.J. Kim, K. Murugesan, J.H. Kim, P.G. Tratnyek, Y.S. Chang, Remediation of trichloroethylene by FeS-coated iron nanoparticles in simulated and real groundwater: effects of water chemistry, *Ind. Eng. Chem. Res.* 52 (2013) 9343–9350.
- [53] D. Turcio-Ortega, D. Fan, P.G. Tratnyek, E. Kim, Y. Chang, Reactivity of Fe/FeS nanoparticles: electrolyte composition effects on corrosion electrochemistry, *Environ. Sci. Technol.* 46 (2012) 12484–12492.
- [54] M. Mangayayam, K. Dideriksen, M. Ceccato, D.J. Tobler, The structure of sulfidized zero valent iron by one-pot synthesis: impact on contaminant selectivity and long-term performance, *Environ. Sci. Technol.* 53 (2019) 4389–4396.
- [55] N.W. Ashcroft, A.R. Denton, Vegard's law, *Phys. Rev. A* 43 (1991) 3161–3164.

- [56] H. Guo, H. Li, K. Jarvis, H. Wan, P. Kunal, S.G. Dunning, Y. Liu, G. Henkelman, S.M. Humphrey, Microwave-assisted synthesis of classically immiscible Ag-Ir alloy nanoparticle catalysts, *ACS Catal.* 8 (2018) 11386–11397.
- [57] Y. Xu, M.A.A. Schoonen, The absolute energy positions of conduction and valence bands of selected semiconducting minerals, *Am. Mineral.* 85 (2000) 543–556.
- [58] Y. Su, A.S. Adeleye, Y. Huang, X. Zhou, A.A. Keller, Y. Zhang, Direct synthesis of novel and reactive sulfide-modified nano iron through nanoparticle seeding for improved cadmium-contaminated water treatment, *Sci. Rep.* 6 (2016) 24358.
- [59] J.F. Moulder, W.F. Stickle, P.E. Sobol, K.D. Bomben, *Handbook of X-ray photoelectron spectroscopy*, Perkin-Elmer, Eden Prairie, 1992.
- [60] S. Johnson, R.J. Madix, Desorption of hydrogen and carbon monoxide from Ni(100), Ni(100)p(2 × 2)S, and Ni(100)c(2 × 2)S surfaces, *Surf. Sci.* 108 (1981) 77–98.
- [61] M.L. Burke, R.J. Madix, Hydrogen on Pd(100)-S: the effect of sulfur on precursor mediated adsorption and desorption, *Surf. Sci.* 237 (1990) 1–19.
- [62] C.H. Bartholomew, P.K. Agrawal, J.R. Katzer, Sulfur poisoning of metals, *Adv. Catal.* 31 (1982) 135–242.
- [63] H. Li, S. Guo, K. Shin, M.S. Wong, G. Henkelman, Design of a Pd-Au nitrite reduction catalyst by identifying and optimizing active ensembles, *ACS Catal.* 9 (2019) 7957–7966.
- [64] V. Tripkovic, T. Vegge, Potential- and rate-determining step for oxygen reduction on Pt(111), *J. Phys. Chem. C* 121 (2017) 26785–26793.
- [65] J. Xu, A. Avellan, H. Li, X. Liu, V. Noël, Z. Lou, Y. Wang, R. Kaegi, G. Henkelman, G. V. Lowry, Sulfur loading and speciation control the hydrophobicity, electron transfer, reactivity, and selectivity of sulfidized nanoscale zerovalent iron, *Adv. Mater.* 32 (2020) 1906910.
- [66] H. Li, K. Shin, G. Henkelman, Effects of ensembles, ligand, and strain on adsorbate binding to alloy surfaces, *J. Chem. Phys.* 149 (2018) 174705.
- [67] Y. Gu, B. Wang, F. He, M.J. Bradley, P.G. Tratnyek, Mechanochemically sulfidated microscale zero valent iron: pathways, kinetics, mechanism, and efficiency of trichloroethylene dechlorination, *Environ. Sci. Technol.* 51 (2017) 12653–12662.
- [68] J. Xu, X. Lv, J. Li, Y. Li, L. Shen, H. Zhou, X. Xu, Simultaneous adsorption and dechlorination of 2, 4-dichlorophenol by Pd/Fe nanoparticles with multi-walled carbon nanotube support, *J. Hazard. Mater.* 225–226 (2012) 36–45.
- [69] Y. Liu, S.A. Majetich, R.D. Tilton, D.S. Sholl, G.V. Lowry, TCE dechlorination rates, pathways, and efficiency of nanoscale iron particles with different properties, *Environ. Sci. Technol.* 39 (2005) 1338–1345.
- [70] A. Nunez Garcia, H.K. Boparai, D.M. O Carroll, Enhanced dechlorination of 1, 2-dichloroethane by coupled nano iron-dithionite treatment, *Environ. Sci. Technol.* 50 (2016) 5243–5251.
- [71] D.W. Elliott, W. Zhang, Field assessment of nanoscale bimetallic particles for groundwater treatment, *Environ. Sci. Technol.* 35 (2001) 4922–4926.
- [72] H. Liu, J. Han, J. Yuan, C. Liu, D. Wang, T. Liu, M. Liu, J. Luo, A. Wang, J.C. Crittenden, Deep dehalogenation of florfenicol using crystalline CoP nanosheet arrays on a Ti plate via direct cathodic reduction and atomic H, *Environ. Sci. Technol.* 53 (2019) 11932–11940.
- [73] Y. Lv, J. Li, Y. Li, L. Liang, H. Dong, K. Chen, C. Yao, Z. Li, J. Li, X. Guan, The roles of pyrite for enhancing reductive removal of nitrobenzene by zero-valent iron, *Appl. Catal. B* 242 (2019) 9–18.
- [74] Y. Liu, T. Phenrat, G.V. Lowry, Effect of TCE concentration and dissolved groundwater solutes on NZVI-promoted TCE dechlorination and H<sub>2</sub> evolution, *Environ. Sci. Technol.* 41 (2007) 7881–7887.
- [75] T. Phenrat, Y. Liu, R.D. Tilton, G.V. Lowry, Adsorbed polyelectrolyte coatings decrease Fe<sup>0</sup> nanoparticle reactivity with TCE in water: conceptual model and mechanisms, *Environ. Sci. Technol.* 43 (2009) 1507–1514.